Highly birefringent optical microfibers

Haifeng Xuan, Jian Ju, Wei Jin*

Department of Electrical Engineering, The Hong Kong Polytechnic University, Hong Kong
**eewjin@polyu.edu.hk*

Abstract: Highly birefringent (Hi-Bi) air-clad silica microfibers (MFs) with wavelength and sub-wavelength scale transverse dimensions are studied theoretically and experimentally. Hi-Bi MFs are taper-drawn from the standard SMF-28 single mode fibers that are "pre-processed" by "cutting away" parts of the silica cladding on opposite sides of the fiber with a femtosecond infrared laser. Such Hi-Bi MFs have approximately elliptical cross-sections and are approximated by a three-layer model comprising a small central Ge-doped region surrounded by an elliptical silica region and an air-cladding. Theoretical modeling shows that phase and group birefringence of the order 10^{-2} can be achieved with such air-clad Hi-Bi MFs. Experiments with an air-clad elliptical fiber with a major diameter of 0.9μm and a minor/major diameter ratio of 0.9 demonstrated a group birefringence of ~ 0.015, agreeing well with the theoretical predictions. The Hi-Bi MFs are useful for micron/nanoscale polarization maintaining transmission and phase-sensitive interferometric sensors.

OCIS codes: (060.2310) Fiber optics; (060.2280) Fiber design and fabrication; (060.2420) Fibers, polarization-maintaining; (230.3990) Micro-optical devices;

References and links

1. R. A. Bergh, H. C. Lefevre, and H. J. Shaw, "An Overview of Fiber-Optic Gyroscopes," J. Lightwave Technol. **2**(2), 91–107 (1984).
2. J. Noda, K. Okamoto, and Y. Sasaki, "Polarization-Maintaining Fibers and Their Applications," J. Lightwave Technol. **4**(8), 1071–1089 (1986).
3. L. Poti, and A. Bogoni, "Experimental demonstration of a PMD compensator with a step control algorithm," IEEE Photon. Technol. Lett. **13**(12), 1367–1369 (2001).
4. T. Hosaka, K. Okamoto, T. Miya, Y. Sasaki, and T. Edahiro, "Low-Loss Single Polarization Fibers with Asymmetrical Strain Birefringence," Electron. Lett. **17**(15), 530–531 (1981).
5. M. P. Varnham, D. N. Payne, R. D. Birch, and E. J. Tarbox, "Single-Polarization Operation of Highly Birefringent Bow-Tie Optical Fibers," Electron. Lett. **19**(7), 246–247 (1983).
6. S. C. Rashleigh, and M. J. Marrone, "Polarization Holding in Elliptical-Core Birefringent Fibers," IEEE J. Quantum Electron. **18**(10), 1515–1523 (1982).
7. R. B. Dyott, J. R. Cozens, and D. G. Morris, "Preservation of polarisation in optical-fibre waveguides with elliptical cores," Electron. Lett. **15**(13), 380–382 (1979).
8. L. M. Tong, R. R. Gattass, J. B. Ashcom, S. L. He, J. Y. Lou, M. Y. Shen, I. Maxwell, and E. Mazur, "Subwavelength-diameter silica wires for low-loss optical wave guiding," Nature **426**(6968), 816–819 (2003).
9. G. Brambilla, V. Finazzi, and D. J. Richardson, "Ultra-low-loss optical fiber nanotapers," Opt. Express **12**(10), 2258–2263 (2004).
10. L. M. Tong, J. Y. Lou, and E. Mazur, "Single-mode guiding properties of subwavelength-diameter silica and silicon wire waveguides," Opt. Express **12**(6), 1025–1035 (2004).
11. J. C. Knight, G. Cheung, F. Jacques, and T. A. Birks, "Phase-matched excitation of whispering-gallery-mode resonances by a fiber taper," Opt. Lett. **22**(15), 1129–1131 (1997).
12. K. J. Vahala, "Optical microcavities," Nature **424**(6950), 839–846 (2003).
13. P. Polynkin, A. Polynkin, N. Peyghambarian, and M. Mansuripur, "Evanescent field-based optical fiber sensing device for measuring the refractive index of liquids in microfluidic channels," Opt. Lett. **30**(11), 1273–1275 (2005).
14. J. Villatoro, and D. Monzon-Hernandez, "Fast detection of hydrogen with nano fiber tapers coated with ultra thin palladium layers," Opt. Express **13**(13), 5087–5092 (2005).
15. X. S. Jiang, L. M. Tong, G. Vienne, X. Guo, A. Tsao, Q. Yang, and D. R. Yang, "Demonstration of optical microfiber knot resonators," Appl. Phys. Lett. **88**(22), 223501 (2006).
16. M. Sumetsky, "Basic elements for microfiber photonics: Micro/nanofibers and microfiber coil resonators," J. Lightwave Technol. **26**(1), 21–27 (2008).

#119946 - $15.00 USD Received 13 Nov 2009; revised 18 Dec 2009; accepted 21 Dec 2009; published 11 Feb 2010

17. S. S. Wang, Z. F. Hu, Y. H. Li, and L. M. Tong, "All-fiber Fabry-Perot resonators based on microfiber Sagnac loop mirrors," Opt. Lett. **34**(3), 253–255 (2009).
18. Y. H. Li, and L. M. Tong, "Mach-Zehnder interferometers assembled with optical microfibers or nanofibers," Opt. Lett. **33**(4), 303–305 (2008).
19. Y. Chen, Z. Ma, Q. Yang, and L. M. Tong, "Compact optical short-pass filters based on microfibers," Opt. Lett. **33**, 2565–2567 (2008).
20. Q. Yang, X. S. Jiang, X. Guo, Y. Chen, and L. M. Tong, "Hybrid structure laser based on semiconductor nanowires and a silica microfiber knot cavity," Appl. Phys. Lett. **94**(10), 101108 (2009).
21. X. S. Jiang, Q. H. Song, L. Xu, J. Fu, and L. M. Tong, "Microfiber knot dye laser based on the evanescent-wave-coupled gain," Appl. Phys. Lett. **90**(23), 233501 (2007).
22. L. M. Tong, J. Y. Lou, R. R. Gattass, S. L. He, X. W. Chen, L. Liu, and E. Mazur, "Assembly of silica nanowires on silica aerogels for microphotonic devices," Nano Lett. **5**(2), 259–262 (2005).
23. I. K. Hwang, Y. H. Lee, K. Oh, and D. N. Payne, "High birefringence in elliptical hollow optical fiber," Opt. Express **12**(9), 1916–1923 (2004).
24. R. B. Dyott, Elliptical fiber waveguides (Artech House, boston.london, 1995).
25. C. Yeh, "Elliptical dielectric waveguides," J. Appl. Phys. **33**(11), 3235–3243 (1962).
26. J. K. Shaw, W. M. Henry, and W. R. Winfrey, "Weakly guiding analysis of elliptical core step index waveguides based on the characteristic numbers of Mathieu's equation," J. Lightwave Technol. **13**(12), 2359–2371 (1995).
27. S. C. Rashleigh, "Measurement of fiber birefringence by wavelength scanning: effect of dispersion," Opt. Lett. **8**(6), 336–338 (1983).
28. X. Chen, M.-J. Li, N. Venkataraman, M. Gallagher, W. Wood, A. Crowley, J. Carberry, L. Zenteno, and K. Koch, "Highly birefringent hollow-core photonic bandgap fiber," Opt. Express **12**(16), 3888–3893 (2004).
29. J. R. Folkenberg, M. D. Nielsen, N. A. Mortensen, C. Jakobsen, and H. R. Simonsen, "Polarization maintaining large mode area photonic crystal fiber," Opt. Express **12**(5), 956–960 (2004).
30. H. F. Xuan, W. Jin, M. Zhang, J. Ju, and Y. B. Liao, "In-fiber polarimeters based on hollow-core photonic bandgap fibers," Opt. Express **17**(15), 13246–13254 (2009).

1. Introduction

Highly birefringent (Hi-Bi) optical fibers that can maintain the state of polarization during light transmission have been widely used in optical fiber sensors, precision optical instruments and optical fiber communication systems [1–3]. Hi-Bi fibers can be produced by introducing stress applying parts around the fiber core, examples of this type of Hi-Bi fibers are the commercial PANDA [4] and Bow-Tie fibers [5]. Alternatively, Hi-Bi operation can be achieved by asymmetric waveguide geometry with elliptical core fibers as a typical representative of this type [6, 7].

Recently, micro/nanofiber photonic devices have attracted significant interest. Optical fibers with diameter of micro/nanometer scale have been taper-drawn from standard optical fibers or glass rods and may potentially be used as low-loss air-clad micro/nanoscale optical waveguides [8, 9]. These air-clad micro/nanofibers have a large external evanescent field [10], allowing strong evanescent wave coupling between them and the environment. Straightforward applications of these thin fibers are waveguide couplers [11, 12] and evanescent wave sensors [13, 14]. A number of micro/nanofiber devices based on evanescent-coupling have been demonstrated, including coiled resonators [15, 16], interferometers [17, 18], filters [19], amplifier and lasers [20, 21]. It has been suggested that micro/nanofibers could function as the basic elements of micro/nanophotonics, which focus on photonic circuits that are composed of micro/nanofibers [8, 22].

However, the micro/nanofibers reported so far are taper-drawn directly from standard signal mode fibers (SMFs) or glass rods. They are typically not Hi-Bi and hence have little or no capability of maintaining the state of polarization during transmission, a crucial factor that determines the stability of phase sensitive devices and sensors.

In this paper, air-clad Hi-Bi microfibers (MFs) with wavelength and sub-wavelength scale diameters are studied theoretically and experimentally. Hi-Bi MFs are fabricated from a standard telecommunication fiber (SMF-28) through a two-step process: firstly, SMF-28 fiber is "pre-processed" by "cutting away" parts of the silica on opposite sides of the cladding with a femtosecond infrared (IR) laser; and then the "pre-processed" fiber is taper-drawn to wavelength/sub-wavelength transverse dimension with a commercial coupler fabrication rig. We show theoretically that phase and group birefringence of the order of 10^{-2} can be achieved with such air-clad Hi-Bi MFs. We measured the birefringence of a Hi-Bi MF with a diameter

#119946 - $15.00 USD Received 13 Nov 2009; revised 18 Dec 2009; accepted 21 Dec 2009; published 11 Feb 2010

of 0.9 μm along the major-axis of the ellipse and obtained a group birefringence of ~0.015, agreeing well with the theoretical prediction.

2. Hi-Bi microfibers: theoretical analysis

It has been shown that large birefringence can be achieved by asymmetric waveguide geometry such as an elliptical core (e-core) [6, 7]. The birefringence of such e-core fibers was shown to grow in proportional to Δn^2, where Δn is the refractive index difference between the core and the cladding [7, 23]. For a traditional e-core fiber comprising a Ge-doped core and silica cladding, the core-cladding index difference Δn is typically less than 0.04. If the silica cladding was replaced by air, which has an index difference of ~0.45 from the doped silica core, the birefringence of the new fiber would be much larger. We propose here to fabricate such air/clad Hi-Bi fibers by a "pre-processing" and then a taper-drawn process as briefed in Section 1 and detailed in Section 3.

Figure 1(a) shows the theoretical model used to study the properties of the air/clad Hi-Bi MFs. The model comprises three layers or regions: an infinite air-cladding, an elliptical core made predominantly of silica with a tiny circular Ge-doped center region. The key waveguide parameters of the fiber are semi-major diameter "*a*" and semi-minor diameter "*b*". The diameter of the Ge-doped region in taper-drawn fiber is very small and can be estimated by $D_{core} \sim (D_{SMF}^{core} / D_{SMF}^{cladding}) * 2a$, where D_{SMF}^{core} and $D_{SMF}^{cladding}$ are respectively the diameters of Ge-doped core and silica cladding of original SMF.

In an elliptical dielectric waveguide, the eigenvalue equations for various modes are no longer defined special function equations as in a circular dielectric waveguide, but a sets of infinite homogenous algebraic equations [24, 25]. In addition, no single order analytic special function representing a single modal field can be found for those boundary conditions, even for a weakly guiding elliptical fiber [24, 26]. In this letter, the waveguide property of the air-clad e-core MFs is numerically investigated by use of a full-vector finite-element method (FEM). During the simulation, the diameter of the air-cladding is set to be 8 times of the major diameter "2*a*". This dimension of air-cladding is found sufficiently large to cause no influence on the dispersion relations of modes. The refractive indices of the air-cladding, the silica and Ge-doped regions are respectively set to $n_{air} = 1$, $n_{silica} = 1.444$, and $n_{Ge-doped} = (1 + 0.36\%) * n_{silica}$.

#119946 - $15.00 USD Received 13 Nov 2009; revised 18 Dec 2009; accepted 21 Dec 2009; published 11 Feb 2010

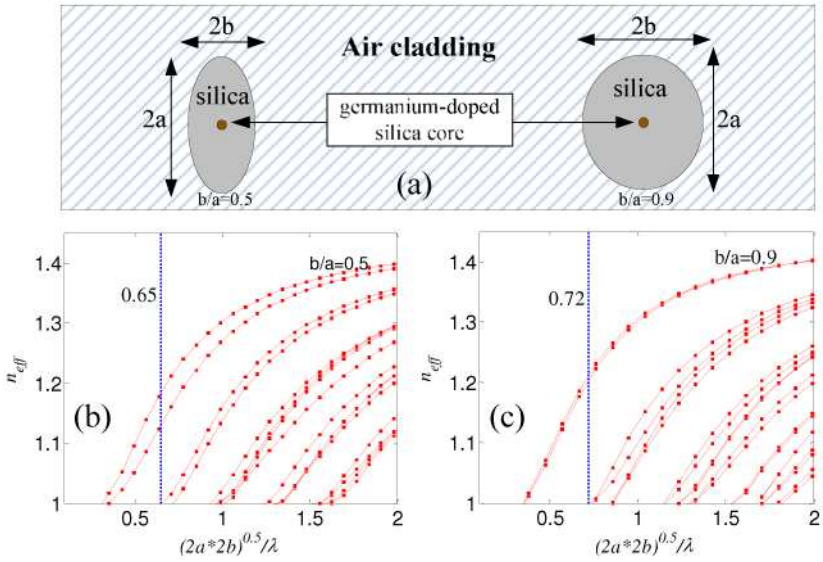

Fig. 1. (a) The three layer model of air-clad elliptical microfiber. Effective indexes of lower-order modes as functions of normalized fiber diameter ($\sqrt{2a*2b}/\lambda$) for *b/a* = 0.5 (b) and *b/a* = 0.9 (c). Vertical dotted lines (blue) in (b) and (c) indicate the critical normalized fiber diameters for higher-order modes cut-off.

Figures 1(b) and 1(c) show respectively the effective refractive indices of the lower order modes as functions of normalized fiber diameter $\sqrt{2a*2b}/\lambda$ for MFs with *b/a* = 0.5 and *b/a* = 0.9, respectively. When the normalized diameter is reduced to a certain value as denoted by the vertical dotted line in Figs. 1(b) and 1(c), only the two non-degenerated HE_{11} (HE_{11}^{x} and HE_{11}^{y}) modes exist, corresponding to the single mode condition of a circular fiber. The cut-off condition in elliptical MFs depends on the ellipticity of the fiber; for example, $\sqrt{2a*2b}/\lambda$ ~0.65 for *b/a* = 0.5 (Fig. 1(b)) and ~0.72 for *b/a* = 0.9 (Fig. 1(c)). $\sqrt{2a*2b}/\lambda$ increases with *b/a* and approaches to the cut-off condition of the circular fiber, i.e., $\sqrt{2a*2b}/\lambda$ ~0.73, when *b/a* is close to 1. Through a series of numerical calculations, we found that, for 0.5 < *b/a* < 1, the higher order modes cut-off condition of the air-clad elliptical MFs can be numerically fitted to the following polynomial:

$$\frac{\sqrt{2a*2b}}{\lambda} = P_{cut-off}\left(\frac{b}{a}\right) = 0.4519*\left(\frac{b}{a}\right)^3 - 1.3181*\left(\frac{b}{a}\right)^2 + 1.3448*\left(\frac{b}{a}\right) + 0.2508 \quad (1)$$

where "*a*" and "*b*" are respectively the semi-major and semi-minor diameters of the fiber, and λ is the optical wavelength in vacuum.

From the Fig. 1(b) and 1(c), it is found that the non-degeneracy of two orthogonal polarization states (HE_{11}^{x} and HE_{11}^{y}) of fundamental HE_{11} mode increases with increasing ellipticity. The non-degeneracy of HE_{11} mode is known as birefringence *B* (phase birefringence) of the optical fiber, and is defined as: $B = n_{eff}^{y} - n_{eff}^{x}$, where the n_{eff}^{x} and n_{eff}^{y} are respectively effective refractive indices of HE_{11}^{x} and HE_{11}^{y} modes.

Figure 2 shows the calculated variations of birefringence as functions of optical wavelength for MFs with various semi-major diameters from 0.2 μm to 5 μm. Figures 2(a) and 2(c) are for *b/a* = 0.5, while Figs. 2(b) and 2(d) are for *b/a* = 0.9. The peak of the birefringence-λ curve red-shifts and becomes broader when the semi-major diameter *a* is varied from 0.2 to 0.8 μm, while the maximum birefringence B_{max} remains at a constant level

#119946 - $15.00 USD Received 13 Nov 2009; revised 18 Dec 2009; accepted 21 Dec 2009; published 11 Feb 2010

for a fixed *b/a* ratio. When the fiber dimension is increased to beyond *a* ~ 1 μm, the birefringence in the wavelength range below 2 μm becomes very small and further decreases with an increase of the fiber diameter, as shown in Figs. 2(c) and 2(d). This is because that the peak birefringence wavelength has been shifted to much longer wavelength. In addition, the MF will become multi-moded for fiber sizes beyond the critical value as predicted by Eq. (1).

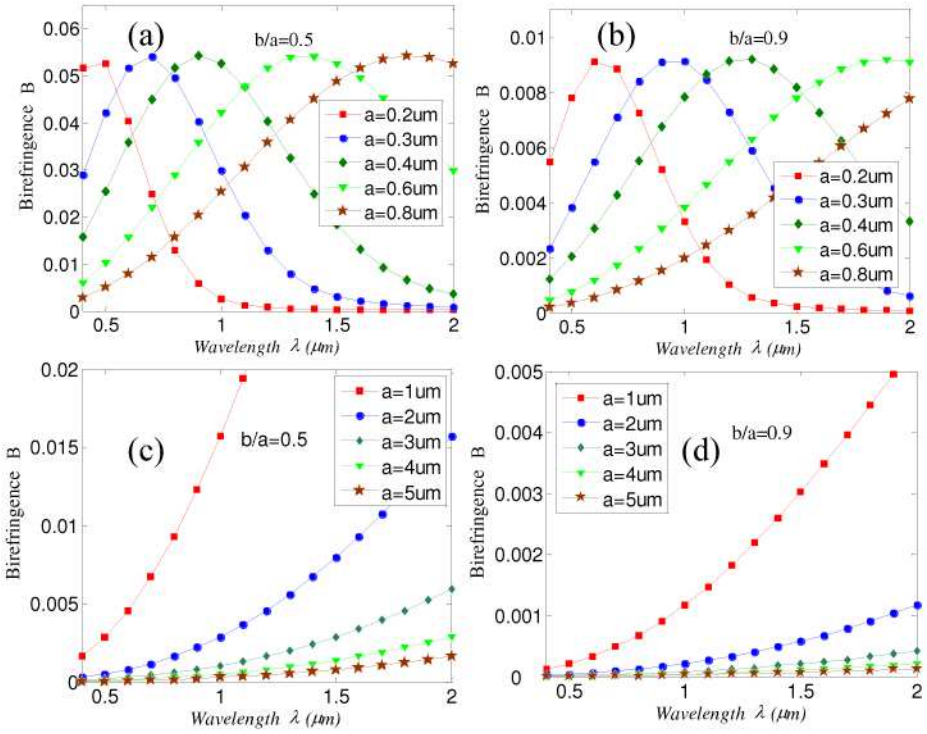

Fig. 2. Birefringence of as function of optical wavelength for various fiber dimensions and ellipticities. (a) *b/a* = 0.5, *a* from 0.2 to 0.8 μm; (b) *b/a* = 0.9, *a* from 0.2 to 0.8 μm; (c) *b/a* = 0.5, *a* from 1 to 5 μm; and (d) *b/a* = 0.9, *a* from 1 to 5 μm

From above observation, it may be concluded that the maximum birefringence B_{max} is independent of the transverse dimension of the fiber but strongly depends on the *b/a* ratio, while the peak birefringence wavelength increases with the fiber transverse dimension. The calculated birefringence as function of normalized fiber diameter ($\sqrt{2a*2b}/\lambda$) with different ellipticity (*b/a* from 0.9 to 0.5) is shown in Fig. 3(a) (the horizontal and the left-vertical axes), while the maximum birefringence B_{max} as a function of *b/a* is shown in the Fig. 3(b). The birefringence of these air-clad elliptical MFs is very high even with a small ellipticity and increases dramatically with an increase of ellipticity. The maximum birefringence B_{max} is ~0.054 for a MF with *b/a* = 0.5 and ~ 0.01 for a MF with *b/a* = 0.9. From the results in Fig. 3(a), the condition for maximum birefringence may be approximated by:

$$\frac{\sqrt{2a*2b}}{\lambda} \sim 0.6 \qquad (2)$$

Equation (2) indicates that, to achieve the maximum birefringence, the transverse dimension of the MF (major diameter "2*a*" and minor diameter "2*b*") should be down to sub-wavelength scale. Furthermore, from Fig. 3(b), the relationship between B_{max} and *b/a* can be numerically fitted by the following polynomial:

#119946 - $15.00 USD Received 13 Nov 2009; revised 18 Dec 2009; accepted 21 Dec 2009; published 11 Feb 2010

$$B_{max} = 0.043946 * (\frac{b}{a})^2 - 0.17444 * (\frac{b}{a}) + 0.13053 \quad (3)$$

The higher order modes cut-off line or single mode condition obtained from the Eq. (1) is also shown in Fig. 3(a) by the "+" line corresponding to horizontal and right-vertical axes. The left side of this line is the single mode operation region in which only the two orthogonal polarizations of the fundamental HE_{11} mode are guided by the fiber. It is obvious that the maximum birefringence for a Hi-Bi MF with *b/a* from 0.5 to 1 always occur in the single mode region. This property is important for Hi-Bi MF design, since the maximum possible birefringence and single mode operation can be achieved at the same time.

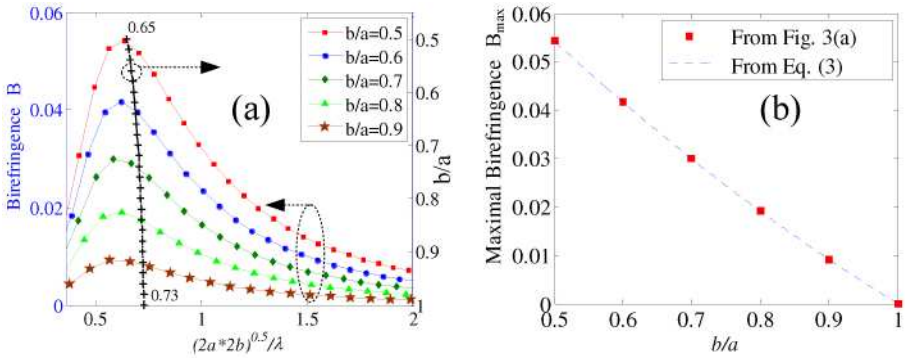

Fig. 3. (a) Birefringence as function of normalized fiber diameter $\sqrt{2a*2b}/\lambda$ for elliptical microfibers with various *b/a* from 0.5 to 0.9 (left-vertical axis). The "+" line (right-vertical axis) is the higher modes cut-off line as determined from Eq. (1); the left side of this line is the single mode region. (b) Maximum birefringence as function of *b/a*.

The importance of the above analysis is that it can be used to design practical air-clad silica Hi-Bi MFs with desired properties. To achieve a target maximum birefringence B_{max} at a particular operating wavelength λ, the fiber parameters and modal property may be estimated by using Eqs. (1) - (3). For example, to obtain a maximum birefringence of B_{max} ~0.01 around center wavelength of 1550 nm, *b/a* can be calculated by using Eq. (3) to be ~0.9; the dimension of the MF can then be determined from Eq. (2) to be *2a* ~ 1 μm. Finally, the higher modes cut-off wavelength of the fiber can be estimated by using Eq. (1) to be ~1.31 μm, meaning that the fiber is single-moded for wavelength beyond 1.31 μm.

3. Hi-Bi microfibers: fabrication

Air-clad Hi-Bi MFs are fabricated from a commercial SMF-28 (outer diameter D ~ 125 μm, core diameter d ~ 8.2 μm, Δn ~ 0.36%) by following a two-step process: firstly, the SMF-28 fiber is "pre-processed" by "cutting away" parts of the silica on opposite sides of the fiber cladding with a femtosecond IR laser, resulting in an rectangle-like cross-section (rectangle with two curved sides) as depicted in Figs. 4(b) and 4(c); then, the "pre-processed" SMF is taper-drawn to wavelength or sub-wavelength scale by using a commercial optical fiber coupler fabrication rig. The cross-sectional shape of the "pre-processed" region was found to retain its rectangle-like shape during initial taper-drawn process and eventually turns to an approximately elliptical shape when the fiber transverse dimension was drawn down to sub-wavelength dimensions. Figure 4 shows the schematic of the femtosecond IR laser setup for "pre-processing" of SMFs. Laser pulses with a wavelength of 800 nm, duration of 120 *fs*, and repetition rate of 1 kHz are produced by a Ti:Sapphire laser. The laser beam is focused onto the SMF by a microscope objective (×10), and the focal spot size is ~3 μm. With the assistance of an optical microscope, the laser focal position is monitored and displayed on a LCD monitor, through which the location of the focal point can be accurately adjusted via a computer controlled translation stage.

#119946 - $15.00 USD Received 13 Nov 2009; revised 18 Dec 2009; accepted 21 Dec 2009; published 11 Feb 2010

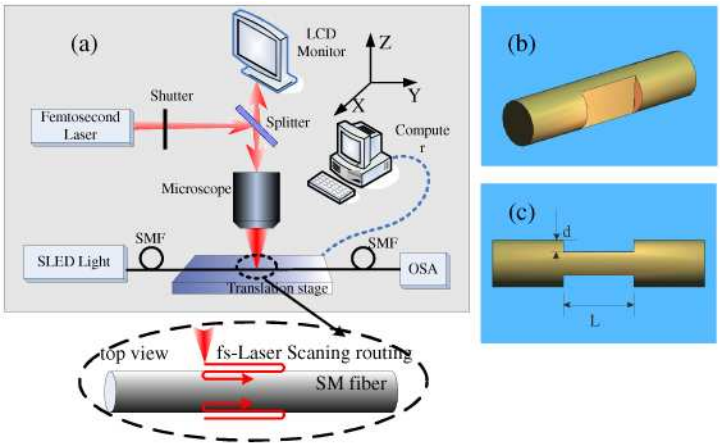

Fig. 4. (a) Schematic of the femtosecond IR laser system for SMF "pre-processing". The femtosecond laser scanning routing is shown in the magnified inset. (b) and (c) Artistic views of the idealized "pre-processed" SMF section from which a Hi-Bi MF may be taper-drawn.

The SMF is mounted on a computer-controlled three-axis translation stage with a tuning resolution of 100 nm. The laser pulses with an irradiation intensity of ~ 20 J/cm^2 are focused onto the one side of the SMF cladding and moved along a pre-programmed track with a speed of 10 μm/s. The detailed routing of femtosecond laser scanning is shown in the magnified inset in Fig. 4(a). Firstly, the focused laser beam scans longitudinally from left to right along the outer-most surface of the fiber for a length of *L*, then the laser beam moves transversely toward the center of the fiber by a step of ~3 μm to perform another longitudinal scanning from right to left. This process is repeated for *N* times to produce, on one side of the fiber, a rectangle shaped groove with depth of *d* (~ *N**3 μm) and a length of *L* as shown in the Fig. 4(c). By following the same routine, a similar groove is created on the opposite side of the fiber. The section of the SMF after "pre-processing" should have a shape similar to that shown in the Figs. 4(b) and 4(c).The depth of "pre-processed" part *d* can be as small as 15 μm to produce microfibers with sufficiently large birefringence.

Figures 5(a) and 5(b) show examples of the SMF sections after femtosecond laser processing. The "pre-processed" SMF samples are taper-drawn to wavelength or sub-wavelength dimension by use of a commercial optical fiber coupler fabrication rig. The SMF is heated and soften by a hydrogen flame which covers about ~ 8 mm length of fiber, much bigger than the length of "pre-processed" fiber section. The large flame width ensures that the whole "pre-processed" region is heated evenly at the beginning of taper-drawing process, which is essential to produce high quality Hi-Bi MFs from the longitudinal non-uniform SMF without breaking the fiber. The flame is scanned along the fiber while the two translation stages holding the fiber are symmetrically moved apart. With our current tapering setup, we can easily fabricate non-circular microfibers with length of ~ 10 mm (the uniform waist region) and diameter down to one micrometer. With optimized fabrication conditions, sub-wavelength fibers with 100 mm in length have been produced [9]. Figures 5(c) and 5(d) show the SEM images of our rectangle-like silica fibers with diameters of the order of 10 μm. Figures 5(e) and 5(f) are samples of elliptical Hi-Bi MFs with wavelength and sub-wavelength dimensions.

#119946 - $15.00 USD Received 13 Nov 2009; revised 18 Dec 2009; accepted 21 Dec 2009; published 11 Feb 2010

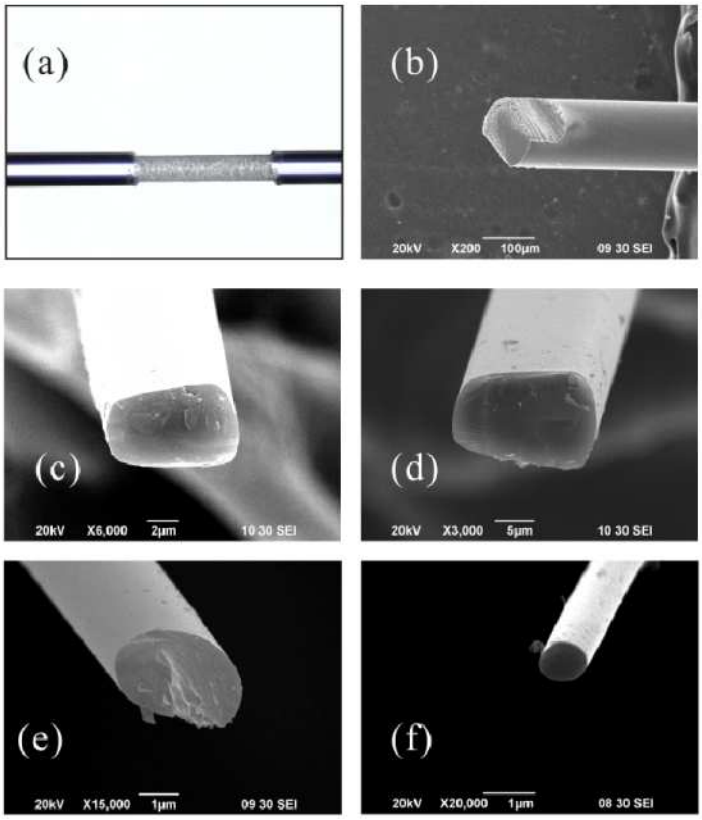

Fig. 5. (a) Microscope image (top view) and (b) SEM image of the SMF section after being "pre-processed" by the femtosecond laser. (c) and (d): SEM images of the rectangle-like silica fibers whose diameters are around 10 µm. (e) and (f): SEM images of elliptical Hi-Bi MFs whose diameters are on the order of ~1 µm. (e) Sample H1. (f) Sample H2. The thin fibers shown in (c) - (f) are taper-drawn from the "pre-processed" SMF.

The transmission property of such fabricated Hi-Bi MF was investigated by using a broadband superluminescent light emitting diode (SLED) and an optical spectrum analyzer (OSA). Figure 6 shows the measured normalized transmitted spectrums of a "pre-processed" SMF before tapering (indicated by dotted blue line) and the taper-drawn Hi-Bi MF drawn from the SMF (solid red line). The normalization was performed against the transmitted spectrum of the same piece of SMF before "pre-proceeding". In fact, the transmitted spectrum of the SMF is continuously monitored during the "pre-processing" of the fiber and the spectrums of the SMF before and after "pre-processing" are found no difference. This is expected because the depth of "cutting away" part is ~ 12% of original cladding, and there should be no substantial influence on the field distribution of core mode. Therefore, no extra loss is introduced by the "pre-processing". For the particular taper-drawn Hi-Bi MF sample shown in Fig. 6, the loss ranges from ~ 1.3 dB at 1450 nm to ~ 0.7 dB at 1650 nm, slightly bigger than a similar circular MFs directly taper-drawn from the SMF28 fiber (< 0.3 dB). One of possible reasons responsible for the relatively high loss may be the surface roughness induced by the femtosecond laser "cutting away" process, which results in irregularities in the MF region and hence larger light scattering out of the MF.

#119946 - $15.00 USD Received 13 Nov 2009; revised 18 Dec 2009; accepted 21 Dec 2009; published 11 Feb 2010

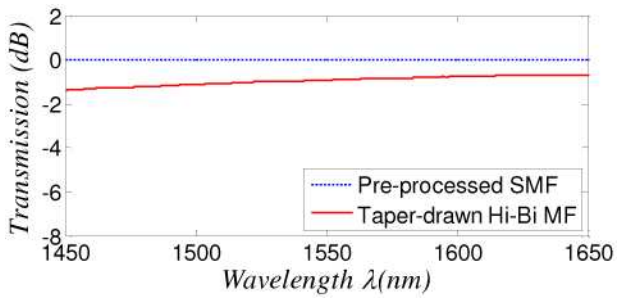

Fig. 6 Normalized transmission spectrum of a Hi-Bi MF with ~1.0 μm major diameter and a minor/major ratio of ~0.9. The tapered region has a central uniform waist region of ~10 mm and transition region of ~35 mm at both sides of the waist.

4. Measurement of polarization properties of Hi-Bi MFs

Direct measurement of the birefringence *B* (phase birefringence) for such thin and short Hi-Bi MFs by using the method [2] for normal-size Hi-Bi fiber is very difficult. However, as have been discussed in Ref. [27-29], the high birefringence of the Hi-Bi MFs can be confirmed by experimentally measuring the group birefringence B_g, which is related to *B* by

$$B_g(\lambda) = B(\lambda) - \lambda \frac{dB(\lambda)}{d\lambda} \tag{4}$$

The group birefringences of Hi-Bi MF samples are measured by a cross polarizer setup with a wavelength scanning technique [27–30]. Light from a broadband source is linearly polarized by the first polarizer, excites two orthogonal polarization modes that propagate through a physical length *L* along a Hi-Bi MF and recombine at the second polarizer. The transmission spectrum measured from an OSA shows periodic oscillations, and the wavelength spacing $\Delta\lambda$ between two adjacent fringe peaks or dips, may be related to the group birefringence B_g by [30]:

$$\Delta\lambda \approx \frac{\lambda^2}{B_g L} \tag{5}$$

Two Hi-Bi MF samples, H1 and H2, both with effective length of ~ 10 mm are examined experimentally. The cross-sections of the two samples are shown respectively in Figs. 5(e) and 5(f). Figures 7(a) and 7(b) show respectively the oscillating transmission spectrum recorded by the OSA. The group birefringences as functions of wavelength are then derived and shown in Figs. 7(c) and 7(d).

The phase birefringence *B* and group birefringence B_g of the fiber samples H1 and H2 are also numerically modeled by using the following parameters: (1) H1, *b/a* = 0.72 and *2a* ~3.4 μm; (2) H2, *b/a* = 0.9 and *2a* ~ 0.9 μm. These parameters are obtained from the SEM images shown in Figs. 5(e) and 5(f). The computed group birefringence B_g and the phase birefringence *B* are also shown in Figs. 7(c) and 7(d). The computed and the measured group birefringences agree well for both samples, indicating the modeling results are reasonably accurate. The phase birefringence *B*, although is not directly experimentally measured, may be regarded to be close to the theoretically computed results shown in Figs. 7(c) and 7(d).

In the wavelength range of Fig. 7, the phase slow axis of H1 (Fig. 7(c)) corresponds to the direction of minor-axis "*a*" (Fig. 1), while the group slow axis is along major-axis "*b*" (i.e., $B_g(\lambda) < 0$). This behavior is due to term $\lambda \cdot dB(\lambda)/d\lambda$ in Eq. (4), which is dominant. For sample H2, the group birefringence B_g and phase birefringence *B* cross at wavelength ~ 1.42

#119946 - $15.00 USD Received 13 Nov 2009; revised 18 Dec 2009; accepted 21 Dec 2009; published 11 Feb 2010

μm (Fig. 7(d)). At the crossing ($B_g = B$), the chromatic dispersion of the phase birefringence is zero ($dB(\lambda)/d\lambda = 0$), meaning that the phase birefringence-wavelength curve has a zero slope. At wavelength beyond ~ 1.42 μm, the chromatic dispersion of the phase birefringence is negative, causing the group birefringence B_g being larger than the phase birefringence B. Below ~ 1.42 μm, the chromatic dispersion of the phase birefringence is positive, and hence B_g is smaller than B. As shown in Fig. 2(b), the phase birefringence of air-clad Hi-Bi MF depends strongly on the wavelength, especially around the two sides of peak birefringence wavelength as determined by the Eq. (2). For the fiber sample H2, the peak birefringence wavelength is ~1.42 μm, while for sample H1, the peak birefringence wavelength is larger than 4 μm, significantly beyond the measurement range (< 1.7 μm). This explains why the difference between group and phase birefringences for the H2 sample is more obvious in the wavelength range than for the H1 sample.

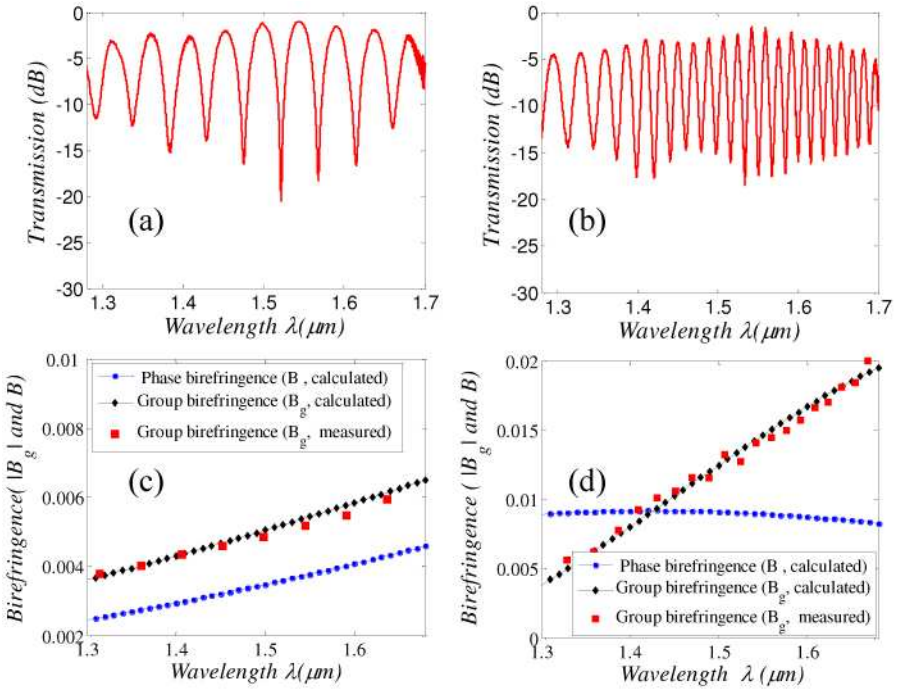

Fig. 7. Measured transmission spectrum for Hi-Bi MF sample (a) H1 and (b) H2. Group birefringence B_g and phase birefringence B as functions of wavelength for Hi-Bi MF sample (c) H1 and (d) H2.

From Fig. 7, it can be seen that the sub-wavelength scale Hi-Bi MF sample H2 has higher birefringence (B_g ~ 0.015 and B close to 0.01 at wavelength of 1.55 μm) even it has a relatively small ellipticity (i.e., b/a = 0.9), while the bigger diameter MF sample H1 has a smaller birefringence within the wavelength of interest, although it has a larger ellipticity (i.e., b/a = 0.72). This confirms that the Hi-Bi MFs can have extraordinarily high birefringence and the dimension of the fiber should be in the sub-wavelength scale in order to achieve the maximum possible birefringence at a given range of operating wavelengths.

The polarization maintaining property of the Hi-Bi MF was also examined experimentally by use of a commercial polarization analyzer (Profile PAT9000B). The PAT9000B kit can be programmed to produce linearly polarized light and polarization direction can be rotated from 0° to 180°. The degree of polarization and the extinction ratio (ER) of the linearly polarized light are, respectively, ~ 99.6% and > 50 dB for every polarization direction. With the

#119946 - $15.00 USD Received 13 Nov 2009; revised 18 Dec 2009; accepted 21 Dec 2009; published 11 Feb 2010

PAT9000B kit, the linearly polarized light can be conveniently aligned to the one of two principal axes of the Hi-Bi fiber. Figure 8(a) shows the polarization state trace obtained from a Hi-Bi MF sample over one hour period in a laboratory environment, when the input polarization is aligned to one of the principal axes of the MF. The sample is ~ 40 cm long with a tapered region of ~ 8 cm and ~ 16 cm SMF pigtails at both sides of the taper. The taper has central uniform waist region of ~10 mm. The waist region has a major diameter of ~ 1.0 μm and a minor/major ratio of ~ 0.9. During experiments, the SMF pigtails were fixed to a stage while the tapered region was loosely suspended in air to allow perturbation of the MF by air-current generated by the air-conditioners in the laboratory. Indeed, we observed significant random movement of the MF during experiment. The output from the MF sample is however a stable linearly polarized light with ER > 20 dB, as shown in Fig. 8(a). The reduced ER, as compared with the input light (~ 50 dB), might be due to the transition regions at both sides of the taper waist. These regions have reduced birefringence but thinner transverse dimension as compared with the SMF pigtails, and hence the polarization state would be more easily affected by the external disturbance. For comparison, a MF sample similar parameters but a circular cross-section was tested and the traced on Poincaré sphere is shown in Fig. 8(b). Obviously the Hi-Bi MF has much better ability for maintaining the linear polarization.

We also repeated the aforementioned two measurements by covering the tapered regions to minimize the effects of disturbance from the air-current and found both measurements give ERs close to 50 dB, indicating the air-current has significan t impact on the polarization state in the thin tapered regions but little effect on the short SMF pigtails which have a large dimension and are fixed to the stage.

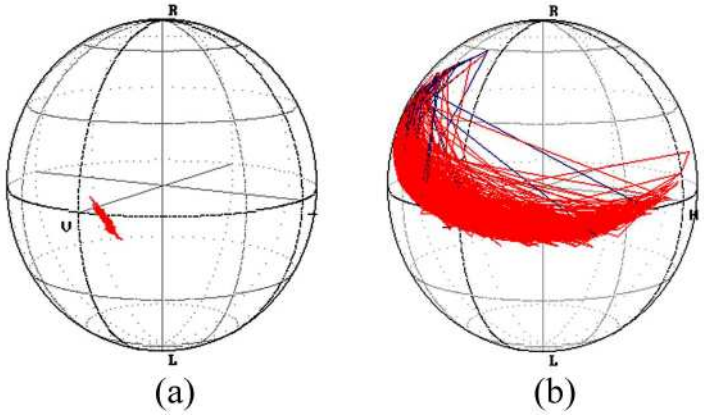

Fig. 8. Poincaré sphere trace for MFs. (a) Hi-Bi MF; and (b) MF with a circular cross-section. The traces were obtained over 1 hour in laboratory environment.

5. Conclusion

Air-clad highly birefringent elliptical-shaped microfibers with transverse dimension down to wavelength and sub-wavelength scale are fabricated and examined theoretically and experimentally. The birefringence of such as microfibers is extraordinarily high and on the order of 10^{-2}. Empirical formulas that relate the higher order mode cutoff and the maximum birefringence with ellipticity (i.e., *b/a*), and that determine peak birefringence wavelength for a given fiber dimension (i.e., *a* and *b*) are obtained. These results will be important for the design of highly birefringent microfibers with desired properties. Potential applications of highly birefringent microfibers include polarization maintaining microfiber couplers, polarization stable microfiber loop resonators and filters, interferometric sensors without polarization fading, and in-line microfiber polarimetric sensors and comb filters.

#119946 - $15.00 USD Received 13 Nov 2009; revised 18 Dec 2009; accepted 21 Dec 2009; published 11 Feb 2010

Acknowledgement

The research work was supported by the Research Grant Council of the Hong Kong SAR Government through a GRF grant PolyU5182/07E., by the NSF of China though grant no: 60629401, and the Hong Kong Polytechnic University through a niche area grant J-BB9K.

#119946 - $15.00 USD Received 13 Nov 2009; revised 18 Dec 2009; accepted 21 Dec 2009; published 11 Feb 2010